

On The Uncertainty Principle of Neural Networks

Jun-Jie Zhang, Dong-Xiao Zhang, Jian-Nan Chen, Long-Gang Pang, and Deyu Meng

Abstract—Despite the successes in many fields, it is found that neural networks are difficult to be both accurate and robust, i.e., high accuracy networks are often vulnerable. Various empirical and analytic studies have substantiated that there is more or less a trade-off between the accuracy and robustness of neural networks. If the property is inherent, applications based on the neural networks are vulnerable with untrustworthy predictions. To more deeply explore and understand this issue, in this study we show that the accuracy-robustness trade-off is an intrinsic property whose underlying mechanism is closely related to the uncertainty principle in quantum mechanics. By relating the loss function in neural networks to the wave function in quantum mechanics, we show that the inputs and their conjugates cannot be resolved by a neural network simultaneously. This work thus provides an insightful explanation for the inevitability of the accuracy-robustness dilemma for general deep networks from an entirely new perspective, and furthermore, reveals a potential possibility to study various properties of neural networks with the mature mathematical tools in quantum physics.

Index Terms—Accuracy-robustness trade-off, adversarial attack, uncertainty principle, quantum physics, deep neural networks.

1 INTRODUCTION

1.1 Background

AN intriguing issue concerning the deep neural networks has garnered significant attentions recently. Despite wide applications in many fields, such as image classification [1], speech recognition [2], playing chess [3] and games [4], predicting protein structures [5], designing chips [6], searching for particles [7], and solving quantum systems [8], [9], etc., these well-trained models are found to be vulnerable under attacks that are imperceptible in terms of human sensations. Overwhelming empirical evidences have manifested that a small non-random perturbation can make a carefully designed neural network give erroneous predictions at a high coincidence [10], [11], [12], [13], [14], [15], [16], [17].

Seeing the fact that more and more researchers are seeking to understand the neural networks, it is crucial for us to further study the accuracy-robustness trade-off of these networks as aforementioned. Meanwhile, since many researchers are using neural networks in their investigations, it is also important for us to explore that if the neural networks are brittle to even small perturbations, which might potentially make applications based on the state-of-the-art deep learning under potential risks. For instance, catastrophic accident may occur on self-driving cars if any imperceptible noises are added on the road signs; medical diagnose can falsely discriminate the cancer cells due to disturbances that the doctors cannot tell by eyes; and personal bank account based on face recognition may be crashed when hacked by small negligible pixels, etc.

To understand the phenomenon, various empirical studies [15], [18], [19] involving different network structures, sizes, performances and even the scales of the training data, do substantiate that there is more or less a trade-off between the accuracy and the robustness of a general neural network. Along with the experimental evidences, theoretical studies [20], [21], [22], [23], ranging from binary classification models to the information theory based analysis, also support the possibility of such trade-off in neural networks. Despite the fact that we still lack a proof to certify these phenomena, many researchers have already begun the concurrent training strategy which optimizes both the robustness and the accuracy of deep neural networks [19], [22], [24], [25], [26], [27], [28], [29].

1.2 Motivation

To the best of our knowledge, the underlying theoretical reason for this accuracy-robustness trade-off is still unknown so far, and it is still not sure whether we can ultimately invent a neural network with both sufficient accuracy and robustness. Therefore, it is of vital importance to clarify the issue, in hope to make all future man-made products relying on the neural networks possibly be predictable and controllable.

Intuitively, it is hard to understand the vulnerability phenomenon since the classical approximation theorems have already shown that a continuous function can be approximated arbitrarily well by a neural network [30], [31], [32], [33]. That is, stable problems described by stable functions should always be solved stably in principle. Therefore, a natural question concerning this issue is to ask whether this accuracy-robustness trade-off is an intrinsic and universal property possessed by general neural networks. If it is purely a matter of neural architecture design and training data acquisition, it is then only needed to concentrate on the designing and training perspectives. If, otherwise, it involves some intrinsic properties which stand at the foundations of deep learning, it is then crucial to further study this trade-off issue in depth.

- J.-J. Zhang, D.-X. Zhang and J.-N. Chen are with the Division of Computational physics and Intelligent modeling, Northwest Institute of Nuclear Technology, Shaanxi, Xi'an 710024, China
E-mail: zjacob@mail.ustc.edu.cn
- L.-G. Pang is with the Key Laboratory of Quark & Lepton Physics of Ministry of Education, Central China Normal University, Wuhan 430079, China.
- D. Meng is with School of Mathematics and Statistics and Ministry of Education Key Lab of Intelligent Networks and Network Security, Xi'an Jiaotong University, Shaanxi, P. R. China.
Email: dymeng@mail.xjtu.edu.cn

1.3 Contribution of this work

In this work, we theoretically show that the accuracy-robustness trade-off of a neural network can be insightfully understood under the uncertainty principle in quantum mechanics, where two complementary factors cannot be measured to an arbitrary high accuracy simultaneously (see derivation in Sec. 3). In terms of neural networks, the uncertainty principle implies that one cannot expect a trained neural network to extract two complementary features of a same input to an arbitrary accuracy. For example, in image classification, if one has trained a network with high accuracy on distinguishing an image class (e.g., dog), this class samples tend to be more easily attacked to enter the domain of other distinguished classes (e.g., car, deer, etc.).

To verify the above statement, we list various experimental evidences both from our attempts and other literatures in Sec. 4. Many experiments with different network structures, datasets, attack strengths as well as loss functions all suggest the inevitable uncertainty principle for general neural networks.

Specifically, our work reveals that neural networks obey the complementarity principle [34] and cannot be both extremely accurate and robust. If we can find out the complementary features of a neural network, we will be able to conduct a concurrent training [25] to possibly achieve a better balance between the accuracy and robustness in the specific applications. Moreover, by introducing the mature mathematics, which has been developed for over 100 years in physics, to the neural networks, we have demonstrated the potential possibility to analyze more intrinsic properties of neural networks in terms of quantum physics.

2 RELEVANT INFORMATION

For the convenience of introducing our main theoretical result, in this section we present some relevant information. Firstly, we introduce one of the most classical and simplest attacking methods, the FGSM attack, as an typical instance to intuitively demonstrate the attacking effect on neural networks. Then, we introduce the necessary knowledge on the uncertainty principle in quantum physics.

2.1 The FGSM attack

One of the most classical and simplest attacking methods is the Fast Gradient Sign Method [21] (FGSM) presented by Goodfellow et al. in 2015. Given a loss function $l(f(X, \theta), Y^*)$, the FGSM creates an attack X by

$$X = X_0 + \epsilon \cdot \text{sign}(\nabla_X l(f(X, \theta), Y^*)|_{X=X_0}), \quad (1)$$

where the loss function l is obtained under a network model $f(X, \theta)$ with parameters θ trained on a pre-collected training dataset, and ϵ is a positive number usually taken to be a small value to make the attack possibly imperceptible. X_0 denotes the raw image to be attacked and classified, and Y^* is the true label for image X_0 . Here, $\nabla_X l(f(X, \theta), Y^*)$ is interpreted as the gradient of l with respect to X . For most of the classifiers, the loss function l is simply the training loss used in training the network. Note that the choice of the loss function does not significantly affect the performance

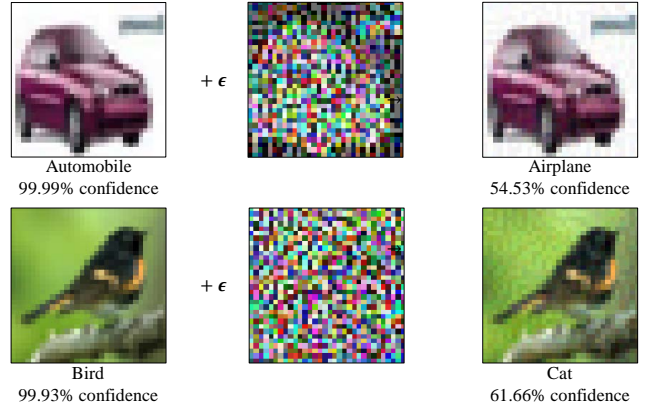


Fig. 1. FGSM attack reduces the test accuracy by adding an imperceptible non-random noise. The trained GoogLeNet on Cifar-10 [35] (see the architecture and implementation in Ref. [36]) gives a 90.78% test accuracy on the test set and only 3.67% robust accuracy under the FGSM attack. The attack is achieved via the transformation $X = X_0 + \epsilon \cdot \text{sign}(\nabla_X l(f(X, \theta), Y^*)|_{X=X_0})$, where X_0 denotes the input images of the training set and X denotes the image to be attacked, $\epsilon = 8/255$ and $\text{sign}(\nabla_X l(f(X, \theta), Y^*)|_{X=X_0})$ gives the non-random noise with $l(f(X, \theta), Y^*)$ denoting the loss function. θ denotes the weights of the trained network.

of the attack [37], [38]. Since the gradient is not difficult to compute for deep neural networks, the attack can always be efficiently implemented.

Fig. 1 depicts the effect of the FGSM attack on two typical images of the Cifar-10 dataset. The trained network correctly identifies the “red car” (X_0 in Eq. (1)) in the left panel as Automobile with a 99.99% confidence, but falsely classifies the attacked one (X in Eq. (1)) on the right panel as Airplane with a 54.53% confidence. Since the two images X_0 and X are imperceptible in terms of human eyes, it is interesting to ask why the neural network fails at identifying them.

2.2 Uncertainty principle in quantum physics

In this subsection, all physical quantities are expressed in the natural unit. In quantum physics, we can describe a particle by a wave packet $\psi(X)$ in the coordinate representation with respect to the coordinate reference frame. The normalization condition for $\psi(X)$ is given by

$$\int |\psi(X)|^2 dX = 1, \quad (2)$$

where the square amplitude $|\psi(X)|^2$ gives the probability density for finding a particle at position $X = (x, y, z)$. To measure the physical quantities of the particle, such as position X and momentum $P = (p_x, p_y, p_z)$, we need to define the position and momentum operators \hat{x}_i and \hat{p}_i as:

$$\begin{aligned} \hat{x}_i \psi(X) &= x_i \psi(X), \\ \hat{p}_i \psi(X) &= -i \frac{\partial}{\partial x_i} \psi(X), \end{aligned} \quad (3)$$

where $i = 1, 2, 3$ denote the x, y, z components in the coordinate space, respectively. The average position and momentum of the particle can be evaluated by

$$\begin{aligned} \langle \hat{x}_i \rangle &= \int \psi^*(X) x_i \psi(X) dX \\ \langle \hat{p}_i \rangle &= \int \psi^*(X) [-i \frac{\partial}{\partial x_i} \psi(X)] dX, \end{aligned} \quad (4)$$

where $\langle \cdot \rangle$ is the Dirac symbol widely used in physics and $\psi^*(X)$ is the complex conjugate of $\psi(X)$. The standard deviations of the position σ_{x_i} and momentum σ_{p_i} are defined respectively as:

$$\begin{aligned}\sigma_{x_i} &= \langle (\hat{x}_i - \langle \hat{x}_i \rangle)^2 \rangle^{1/2}, \\ \sigma_{p_i} &= \langle (\hat{p}_i - \langle \hat{p}_i \rangle)^2 \rangle^{1/2}.\end{aligned}\quad (5)$$

In the year of 1927, Heisenberg introduced the first formulation of the uncertainty principle in his German article [39]. The Heisenberg's uncertainty principle asserts a fundamental limit to the accuracy for certain pairs. Such variable pairs are known as complementary variables (or canonically conjugate variables). The formal inequality relating the standard deviation of position σ_{x_i} and the standard deviation of momentum σ_{p_i} reads

$$\sigma_{x_i} \sigma_{p_i} \geq \frac{1}{2}.\quad (6)$$

Uncertainty relation Eq. (6) states a fundamental property of quantum systems and can be understood in terms of the Niels Bohr's complementarity principle [34]. That is, objects have certain pairs of complementary properties cannot be observed or measured simultaneously.

3 UNCERTAINTY PRINCIPLE FOR NEURAL NETWORKS

3.1 Formulas and notations for neural networks

Without loss of generality, we can assume that the loss function $l(f(X, \theta), Y)$ is square integrable¹,

$$\int l(f(X, \theta), Y)^2 dX = \beta.\quad (7)$$

Eq. (7) allows us to further normalize the loss function as

$$\psi_Y(X) = \frac{l(f(X, \theta), Y)}{\beta^{1/2}},\quad (8)$$

so that

$$\int \psi_Y(X)^2 dX = 1.\quad (9)$$

For convenience, we refer $\psi_Y(X)$ as a neural packet in the later discussions. Note that under different labels Y , a neural network will be with a set of neural packets.

An image $X = (x_1, \dots, x_i, \dots, x_M)$ with M pixels can be seen as a point in the multi-dimensional space, where the numerical values of $(x_1, \dots, x_i, \dots, x_M)$ correspond to the pixel values. The pixel and attack operators of the neural packet $\psi_Y(X)$ can then be defined as:

$$\begin{aligned}\hat{x}_i \psi_Y(X) &= x_i \psi_Y(X), \\ \hat{p}_i \psi_Y(X) &= \frac{\partial}{\partial x_i} \psi_Y(X).\end{aligned}\quad (10)$$

Similar as Eq. (4), the average pixel value at x_i associated with neural packet $\psi_Y(X)$ can be evaluated as

$$\langle \hat{x}_i \rangle = \int \psi_Y^*(X) x_i \psi_Y(X) dX.\quad (11)$$

1. In practical applications, it is rational to only consider the loss function in a limited range $l(f(X, \theta), Y) < C$ under a large constant C , since samples out of this range can be seen as outliers and meaningless to the problem. The loss function can then be generally guaranteed to be square integrable in this functional range.

Since $\psi_Y(X)$ corresponds to a purely real number without imaginary part, the above equation is equivalent to:

$$\langle \hat{x}_i \rangle = \int \psi_Y(X) x_i \psi_Y(X) dX.\quad (12)$$

Besides, the attack operator $\hat{p}_i = \frac{\partial}{\partial x_i}$ corresponds to the conjugate variable of x_i . And we can obtain the average value for \hat{p}_i as

$$\langle \hat{p}_i \rangle = \int \psi_Y(X) \frac{\partial}{\partial x_i} \psi_Y(X) dX.\quad (13)$$

3.2 Derivation of the uncertainty relation

The uncertainty principle of a trained neural network can then be deduced by the following theorem:

Theorem 1. *The standard deviations σ_{p_i} and σ_{x_i} corresponding to the attack and pixel operators \hat{p}_i and \hat{x}_i , respectively, are restricted by the relation:*

$$\sigma_{p_i} \sigma_{x_i} \geq \frac{1}{2}.\quad (14)$$

Proof. We first introduce the standard deviations σ_a and σ_b corresponding to two general operators \hat{A} and \hat{B} . Then it follows that:

$$\sigma_a \sigma_b = \langle (\hat{A} - \langle \hat{A} \rangle)^2 \rangle^{1/2} \langle (\hat{B} - \langle \hat{B} \rangle)^2 \rangle^{1/2} \equiv \langle \hat{a}^2 \rangle^{1/2} \langle \hat{b}^2 \rangle^{1/2}.\quad (15)$$

In general, for any two unbounded real operators $\langle \hat{a} \rangle$ and $\langle \hat{b} \rangle$, the following relation holds

$$0 \leq \langle (\hat{a} - i\hat{b})^2 \rangle = \langle \hat{a}^2 \rangle - i\langle \hat{a}\hat{b} - \hat{b}\hat{a} \rangle + \langle \hat{b}^2 \rangle.\quad (16)$$

If we further replace \hat{a} and \hat{b} in Eq. (16) by operators $\hat{a}\langle \hat{a}^2 \rangle^{-1/2}$ and $\hat{b}\langle \hat{b}^2 \rangle^{-1/2}$, we can then obtain the property $2\langle \hat{a}^2 \rangle^{1/2} \langle \hat{b}^2 \rangle^{1/2} \geq i\langle \hat{a}\hat{b} - \hat{b}\hat{a} \rangle$, which gives the basic bound for the commutator $[\hat{a}, \hat{b}] \equiv \hat{a}\hat{b} - \hat{b}\hat{a}$,

$$\langle \hat{a}^2 \rangle^{1/2} \langle \hat{b}^2 \rangle^{1/2} \geq |i\frac{1}{2}\langle [\hat{a}, \hat{b}] \rangle|.\quad (17)$$

Seeing the fact that $[\hat{a}, \hat{b}] = [\hat{A}, \hat{B}]$, we finally obtain the uncertainty relation

$$\sigma_a \sigma_b \geq |i\frac{1}{2}\langle [\hat{A}, \hat{B}] \rangle|.\quad (18)$$

In terms of the neural networks, we can simply replace operators \hat{A} and \hat{B} by \hat{p}_i and \hat{x}_i introduced in Eq. (10), and this leads to

$$\sigma_{p_i} \sigma_{x_i} \geq |i\frac{1}{2}\langle [\hat{p}_i, \hat{x}_i] \rangle| = \frac{1}{2},\quad (19)$$

where we have used the relation

$$\begin{aligned}[\hat{p}_i, \hat{x}_i] \psi_Y(X) &= [\hat{p}_i \hat{x}_i - \hat{x}_i \hat{p}_i] \psi_Y(X) \\ &= \frac{\partial}{\partial x_i} [x_i \psi_Y(X)] \\ &\quad - x_i \frac{\partial}{\partial x_i} \psi_Y(X) \\ &= \psi_Y(X).\end{aligned}\quad (20)$$

□

TABLE 1
Comparison of the uncertainty principle between quantum physics and neural networks.

Quantum physics		Neural networks	
position	$X = (x, y, z)$	$X = (x_1, \dots, x_i, \dots, x_M)$	image (input)
momentum (conjugate of position)	$P = (p_x, p_y, p_z)$	$P = (p_1, \dots, p_i, \dots, p_M)$	attack (conjugate of input)
wave function	$\psi(X)$	$\psi_Y(X)$	normalized loss function (neural packet)
normalize condition	$\int \psi(X) ^2 dX = 1$	$\int \psi_Y(X) ^2 = 1$	normalize condition
position operator	$\hat{x}_i \psi(X) = x_i \psi(X)$	$\hat{x}_i \psi_Y(X) = x_i \psi_Y(X)$	pixel operator
momentum operator	$\hat{p}_i \psi(X) = -i \frac{\partial}{\partial x_i} \psi(X)$	$\hat{p}_i \psi_Y(X) = \frac{\partial}{\partial x_i} \psi_Y(X)$	attack operator
standard deviation for measuring position	$\sigma_{x_i} = \langle (\hat{x}_i - \langle \hat{x}_i \rangle)^2 \rangle^{1/2}$	$\sigma_{x_i} = \langle (\hat{x}_i - \langle \hat{x}_i \rangle)^2 \rangle^{1/2}$	standard deviation for resolving pixel
standard deviation for measuring momentum	$\sigma_{p_i} = \langle (\hat{p}_i - \langle \hat{p}_i \rangle)^2 \rangle^{1/2}$	$\sigma_{p_i} = \langle (\hat{p}_i - \langle \hat{p}_i \rangle)^2 \rangle^{1/2}$	standard deviation for resolving attack
uncertainty relation	$\sigma_{x_i} \sigma_{p_i} \geq \frac{1}{2}$	$\sigma_{x_i} \sigma_{p_i} \geq \frac{1}{2}$	uncertainty relation

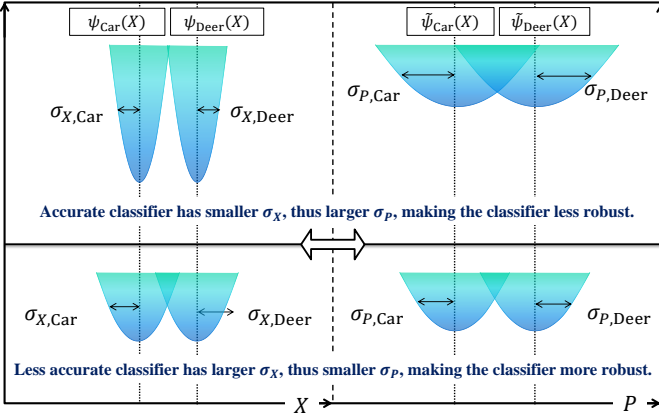


Fig. 2. Schematic illustration of the uncertain relation in binary classification. $\psi_{\text{Car}}(X)$ and $\psi_{\text{Deer}}(X)$ denote the normalized loss functions; $\tilde{\psi}_{\text{Car}}(X)$ and $\tilde{\psi}_{\text{Deer}}(X)$ denote the corresponding conjugates.

Note that for a trained neural network, $\psi_Y(X)$ depends on the dataset and the structure of the network.

Eq. (19) is a general result for general neural networks (see extension to the generation network in supplementary material). For convenience, we compare the formulas in quantum physics with those used in neural networks in Tab. 1 to facilitate easy understandings for readers.

3.3 Understanding the uncertainty principle

To understand how Eq. (19) leads to the trade-off of accuracy and robustness, we consider an example of a binary classifier which distinguishes two categories, e.g., Car and Deer. In Fig. 2, we schematically plot the neural packets $\psi_{\text{Car}}(X)$ and $\psi_{\text{Deer}}(X)$ in the representation of the pixel variable X , as well as their corresponding conjugates. Here the attack operators are denoted as $P = (\hat{p}_1, \dots, \hat{p}_i, \dots, \hat{p}_M)$.

Images X can be seen as vectors in the high dimensional space. The neural packets map the images into scalar values. The two separated functions in the left panel represent the neural packets of the two classes after training. A higher test accuracy is expected if the standard deviations $\sigma_{X,\text{Car}}$ and $\sigma_{X,\text{Deer}}$ are small, so that the two neural packets can be more easily separated apart (as shown in the upper left panel). In the upper right panel, restricted by the uncertainty relation shown in Eq. (19), $\sigma_{P,\text{Car}}$ and $\sigma_{P,\text{Deer}}$ are inevitably larger, inclining to more possibly conduct an overlap between the neural packets in P . On the other hand, if $\sigma_{X,\text{Car}}$ and $\sigma_{X,\text{Deer}}$ are relatively larger, the trained network tends to be less accurate, while simultaneously leading to a smaller overlapped region between neural packets in P , as illustrated in the lower panel of Fig. 2.

In the FGSM attack, the attacked image is of the form:

$$\begin{aligned}
 X &= X_0 + \epsilon \cdot \text{sign}(\nabla_X l(f(X, \theta), Y^*)|_{X=X_0}) \\
 &\sim X_0 + \epsilon \cdot \nabla_X l(f(X, \theta), Y^*)|_{X=X_0} \\
 &= X_0 + \epsilon \cdot \nabla_X [\beta^{1/2} \psi_{Y^*}(X_0)] \\
 &= X_0 + \epsilon' \hat{P} \psi_{Y^*}(X_0),
 \end{aligned} \tag{21}$$

where $\hat{P} = (\frac{\partial}{\partial x_1}, \dots, \frac{\partial}{\partial x_i}, \dots, \frac{\partial}{\partial x_M})$ and $\epsilon' = \epsilon \cdot \beta^{1/2}$. In the second line of Eq. (21) we have used the property substantiated in [40]: "even without the 'Sign' of the FGSM, a successful attack can also be achieved". From Eq. (21), we can then obtain

$$\hat{P} \psi_{Y^*}(X_0) \sim \epsilon' / \epsilon \cdot \text{sign}(\nabla_X l(f(X, \theta), Y^*)|_{X=X_0}), \tag{22}$$

which is the reason that we call \hat{p}_i the attack operator. In the upper panel of Fig. 2, we know that the two neural packets tend to overlap in P under small $\sigma_{X,\text{Car}}$ and $\sigma_{X,\text{Deer}}$. Therefore, in such circumstances, a successful attack tends more possibly to occur.

TABLE 2

Test and robust accuracies for different classifiers on MNIST dataset.

Network type	Test accuracy (%)			Robust accuracy (%)		
	N_{epoch}			N_{epoch}		
	1	30	50	1	30	50
ConvNet	97.31	98.71	98.72	41.44	50.98	53.74
ResNet	98.65	99.50	99.57	90.88	98.22	98.27
YGCNN	97.35	99.15	99.19	59.84	49.06	45.68

TABLE 3

Test and robust accuracies for different classifiers on Cifar-10 dataset.

Network type	Test accuracy (%)			Robust accuracy (%)		
	N_{epoch}			N_{epoch}		
	1	5	50	1	5	50
ConvNet	45.71	60.46	63.07	12.49	6.62	2.88
ResNet	70.42	82.97	86.86	10.67	14.17	1.45
GoogleNet	67.71	81.18	86.61	10.64	8.44	0.08

4 NUMERICAL EVIDENCES FOR THE UNCERTAINTY PRINCIPLE

4.1 Numerical experimental results

To verify the proposed uncertainty principle, we use four different networks, including Convolutional (ConvNet) [41], [42], [43], Residual (ResNet) [44], Google (GoogleNet) [45] and YGCNN [46], as the classifiers. ConvNet, ResNet and GoogleNet are used for Cifar-10 dataset and ConvNet, ResNet and YGCNN are applied on MNIST dataset. The four networks are trained at various epoch numbers N_{epoch} . Since the network structures are standard, we refer readers to Ref. [36] for more implementation details.

Here the test accuracy (TA) is calculated as the classification accuracy on the test data, and the robust accuracy (RA) is obtained by applying the trained classifiers on the attacked images on the test data. The attack is implemented by employing the Projected Gradient Descent (PDG) method [47], [48], which is considered as one of the most effective ways to achieve moderate adversarial attacks. Inspired by FGSM, PDG performs an iterative attack via

$$X_{n+1} = \text{Clip}_{\epsilon} \{ X_n + \alpha \cdot \text{sign}(\nabla_X l(f(X, \theta), Y^*)|_{X=X_n}), \quad (23)$$

where Clip_{ϵ} refers to a truncation which limits the data in range $[-\epsilon, \epsilon]$. For the MNIST dataset the attack strength α and clamp bound ϵ are set to be 0.025 and 0.1, and for Cifar-10 they are specified as $\alpha = 2/255$ and $\epsilon = 8/255$. All test images are attacked iteratively for 4 steps with l_{∞} loss.

Since the uncertainty relation provides a lower bound on the standard deviations, we are able to increase TA and RA simultaneously if the lower bound is not reached. This condition is shown by the result of ConvNet and ResNet in Tab. 2 (for clarity, we have set these values in bold and italic font), where we present the obtained TA and RA on the MNIST dataset. If the lower bound is approximately reached, as shown by the result of YGCNN, the uncertainty

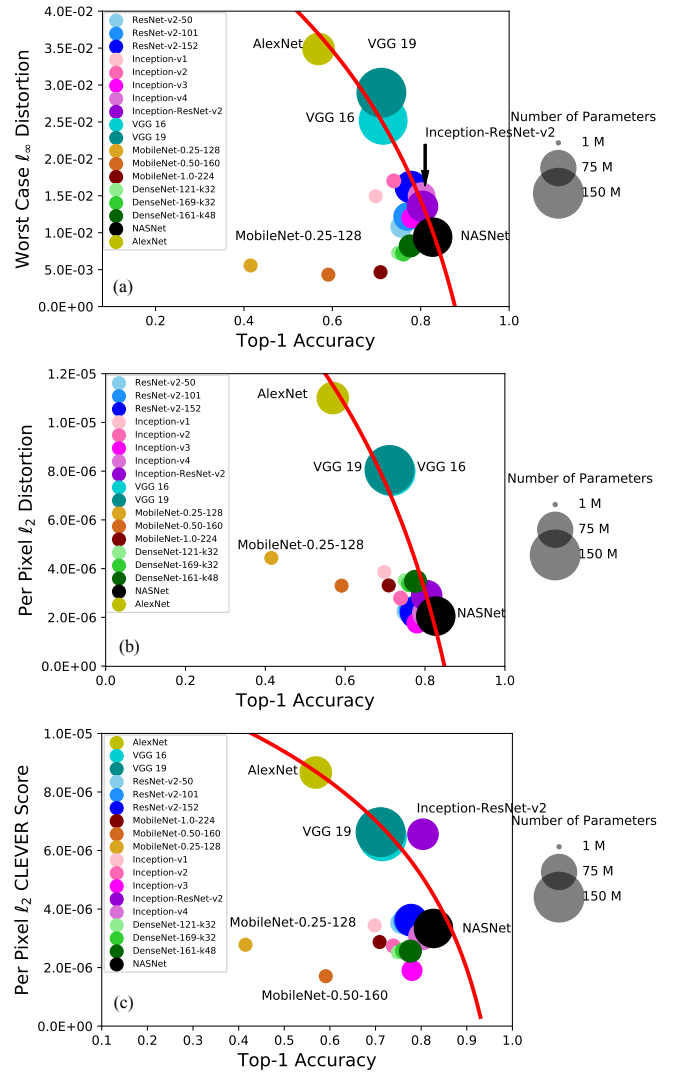


Fig. 3. Robustness vs. classification accuracy of I-FGSM attack, $C\&W$ attack and CLEVER score on random targets over 18 ImageNet models. (a) Fitted Pareto frontier of l_{∞} distortion (I-FGSM attack) vs. top-1 accuracy. (b) Fitted Pareto frontier of l_2 distortion ($C\&W$ attack) vs. top-1 accuracy. (c) Fitted Pareto frontier of l_2 CLEVER score vs. top-1 accuracy. More details of these attacks are demonstrated in Ref. [18].

relation will pose a limit on TA and RA. Thus, we see that an increase in TA corresponds to a decrease in RA. Note that higher TA does not necessarily implies that the trained network with neural packet $\psi_{Y^*}(X)$ has reached the lower bound. As mentioned in Subsec. 3.2, the neural packet $\psi_{Y^*}(X)$ depends on the dataset and the network architecture. Thus, different network structures and datasets may behave differently. This can rationally explain that even though TA for ResNet is larger than that of YGCNN, we can still improve its TA and RA simultaneously. The similar phenomenon can also be observed on Cifar-10 dataset, which can be seen in Tab. 3, where an increase in TA corresponds to a decrease in RA.

4.2 Accuracy-robustness trade-off on 18 different deep classification models

Actually, the aforementioned accuracy-robustness trade-off has been widely observed in current literatures on

image classification as well as other neural network based applications. Here, as a complement, we report one of such comprehensive studies on 18 deep classification models raised in [18]. For other related empirical studies, readers can refer to Refs. [15], [16], [19], [20], [21], [22], [24], [29].

In [18], TA is measured by the Top-1 accuracy on ImageNet dataset, and RA is measured by three different metrics: the worst case l_∞ distortion, per pixel l_2 distortion and per pixel l_2 CLEVER score. Higher RA values correspond to more robust models. Fig. 3 shows the obtained results on 18 different networks with different attacking methods in this literature. In general, an increase in TA evidently corresponds to a decrease in RA. The tendency is not sensitive to the specific attacking methods adopted. Meanwhile, the networks of a same family, e.g., VGG, Inception Nets, ResNets, and DenseNets, share similar robustness properties. Since the uncertainty relation depends on both the network structure and dataset, the reported results in [18] is consistent with the proposed uncertainty principle, and thus also provides an evidence to support the rationality of our result.

5 CONCLUSION AND DISCUSSION

In this study, we have found that for a classifier to be both accurate and robust, it needs to resolve the features of both the input and its conjugate, which is restricted by the uncertainty relation expressed as Eq. (19). The underlying mathematics of the uncertainty principle for neural networks is equivalent to that used in the quantum theory, indicating that the uncertainty relation is an intrinsic property for general neural networks. This exploration should be beneficial in inspiring more attentions to be paid to the vulnerability of neural networks, especially in current days when this issue has been widely exposed due to the growing needs in the applications of neural networks.

Meanwhile, our work reveals that the mathematics in quantum physics could be potentially extended to reveal the insightful properties of neural networks. In quantum physics, as long as we specify the wave function $\psi(X)$, we can study the relevant properties of the physical state following a set of mature mathematical procedures. Similarly, since we have directly converted the loss function into neural packets, it is possible to use the analytical tools in quantum physics to study neural networks.

There are also possible effective conjugates in other adversarial attacks beyond those attempted in this study. In Tab. 4, we list some of the typical attacking methods and their conjugates that probably make them successful attack. Although we still cannot give the conjugates of the black-box attacks [52], [53] explicitly, these methods should possibly map the distribution functions of the datasets to the overlapped ones as shown in Fig. 2. We will make efforts to investigate this issue in our future research.

ACKNOWLEDGMENTS

We thank Prof. David Donoho from Stanford University for providing valuable suggestions on the accuracy robustness of neural networks. Many thanks are given to Prof. Tai-Jiao Du, Prof. Hai-Yan xie, Prof. Yin-Jun Gao and Prof. Guo-Liang Peng from Northwest Insitute of Nuclear Technology

for their funding and support of the work. The work is partly supported by the National Natural Science Foundation of China (NSFC) under the grant number 12105227 and the National Key Research and Development Program of China under Grant No. 2020YFA0709800.

REFERENCES

- [1] A. Krizhevsky, I. Sutskever, and G. E. Hinton, "Imagenet classification with deep convolutional neural networks," *Commun. ACM*, vol. 60, no. 6, pp. 84–90, may 2017.
- [2] G. Hinton, L. Deng, D. Yu, G. E. Dahl, A.-r. Mohamed, N. Jaitly, A. Senior, V. Vanhoucke, P. Nguyen, T. N. Sainath, and B. Kingsbury, "Deep neural networks for acoustic modeling in speech recognition: The shared views of four research groups," *IEEE Signal Processing Magazine*, vol. 29, no. 6, pp. 82–97, 2012.
- [3] D. Silver, A. Huang, C. J. Maddison, A. Guez, L. Sifre, G. van den Driessche, J. Schrittwieser, I. Antonoglou, V. Panneershelvam, M. Lanctot, S. Dieleman, D. Grewe, J. Nham, N. Kalchbrenner, I. Sutskever, T. Lillicrap, M. Leach, K. Kavukcuoglu, T. Graepel, and D. Hassabis, "Mastering the game of go with deep neural networks and tree search," *Nature*, vol. 529, no. 7587, pp. 484–489, jan 2016.
- [4] J. Schrittwieser, I. Antonoglou, T. Hubert, K. Simonyan, L. Sifre, S. Schmitt, A. Guez, E. Lockhart, D. Hassabis, T. Graepel, T. Lillicrap, and D. Silver, "Mastering atari, go, chess and shogi by planning with a learned model," *Nature*, vol. 588, no. 7839, pp. 604–609, dec 2020.
- [5] A. W. Senior, R. Evans, J. Jumper, J. Kirkpatrick, L. Sifre, T. Green, C. Qin, A. Židek, A. W. R. Nelson, A. Bridgland, H. Pedones, S. Petersen, K. Simonyan, S. Crossan, P. Kohli, D. T. Jones, D. Silver, K. Kavukcuoglu, and D. Hassabis, "Improved protein structure prediction using potentials from deep learning," *Nature*, vol. 577, no. 7792, pp. 706–710, jan 2020.
- [6] A. Mirhoseini, A. Goldie, M. Yazgan, J. W. Jiang, E. Songhori, S. Wang, Y.-J. Lee, E. Johnson, O. Pathak, A. Nazi, J. Pak, A. Tong, K. Srinivasa, W. Hang, E. Tuncer, Q. V. Le, J. Laudon, R. Ho, R. Carpenter, and J. Dean, "A graph placement methodology for fast chip design," *Nature*, vol. 594, no. 7862, pp. 207–212, jun 2021.
- [7] P. Baldi, P. Sadowski, and D. Whiteson, "Searching for exotic particles in high-energy physics with deep learning," *Nature Communications*, vol. 5, no. 1, jul 2014.
- [8] G. Carleo and M. Troyer, "Solving the quantum many-body problem with artificial neural networks," *Science*, vol. 355, no. 6325, pp. 602–606, 2017. [Online]. Available: <https://www.science.org/doi/abs/10.1126/science.aag2302>
- [9] L.-G. Pang, K. Zhou, N. Su, H. Petersen, H. Stöcker, and X.-N. Wang, "An equation-of-state-meter of quantum chromodynamics transition from deep learning," *Nature Communications*, vol. 9, no. 1, jan 2018.
- [10] C. Szegedy, W. Zaremba, I. Sutskever, J. Bruna, D. Erhan, I. Goodfellow, and R. Fergus, "Intriguing properties of neural networks," in *2nd International Conference on Learning Representations, ICLR 2014*, Jan. 2014.
- [11] K. Eykholt, I. Evtimov, E. Fernandes, B. Li, A. Rahmati, C. Xiao, A. Prakash, T. Kohno, and D. Song, "Robust physical-world attacks on deep learning visual classification," in *2018 IEEE/CVF Conference on Computer Vision and Pattern Recognition*, 2018, pp. 1625–1634.
- [12] R. Jia and P. Liang, "Adversarial examples for evaluating reading comprehension systems," in *Proceedings of the 2017 Conference on Empirical Methods in Natural Language Processing*. Copenhagen, Denmark: Association for Computational Linguistics, Sep. 2017, pp. 2021–2031. [Online]. Available: <https://aclanthology.org/D17-1215>
- [13] H. Chen, H. Zhang, P.-Y. Chen, J. Yi, and C.-J. Hsieh, "Attacking visual language grounding with adversarial examples: A case study on neural image captioning," *Proceedings of the 2017 Conference on Empirical Methods in Natural Language Processing*, pp. 2587–2597, 2018.
- [14] N. Carlini and A. D. Wagner, "Audio adversarial examples: Targeted attacks on speech-to-text," *2018 IEEE Symposium on Security and Privacy Workshops (SPW 2018)*, pp. 1–7, 2018.
- [15] H. Xu, C. Caramanis, and S. Mannor, "Sparse algorithms are not stable: A no-free-lunch theorem," *IEEE Trans. Pattern Anal. Mach. Intell.*, pp. 187–193, 2012.

TABLE 4
Possible effective conjugates of some attacking methods.

Attack method	Attack procedure	Possible effective conjugates
One-step target class [47]	$X^{\text{adv}} = X - \epsilon \text{sign}(\nabla_X l(f(X, \theta), y_{\text{target}}))$	$\epsilon \text{sign}(\nabla_X l(f(X, \theta), y_{\text{target}}))$
Basic iterative [47]	$X_0^{\text{adv}} = X,$ $X_{N+1}^{\text{adv}} = \text{Clip}_{X, \epsilon} \{X_N^{\text{adv}} + \alpha \text{sign}(\nabla_X l(f(X_N^{\text{adv}}, \theta), y_{\text{True}}))\}$	$\alpha \text{sign}(\nabla_X l(f(X_N^{\text{adv}}, \theta), y_{\text{True}}))$
Iterative least-likely class [47]	$X_0^{\text{adv}} = X,$ $X_{N+1}^{\text{adv}} = \text{Clip}_{X, \epsilon} \{X_N^{\text{adv}} - \alpha \text{sign}(\nabla_X l(f(X_N^{\text{adv}}, \theta), y_{\text{LL}}))\}$	$\alpha \text{sign}(\nabla_X l(f(X_N^{\text{adv}}, \theta), y_{\text{LL}}))$
Jacobian Saliency Map Attack [49]	$X^{\text{adv}} = X + \delta_X, \text{argmin}_{\delta_X} \ \delta_X\ \text{ s.t. } F(X + \delta_X) = Y^*,$ a term $S = \text{saliency_map}(\nabla F(X^*, \Gamma, Y^*))$ is evaluated when finding δ_X	$\text{saliency_map}(\nabla F(X^*, \Gamma, Y^*))$
DeepFool [50]	$X^{\text{adv}} = X + \sum_i r_i, r_i = \frac{ l'_i }{\ \omega'_i\ _2} \omega'_i.$ When evaluating ω'_i , a term $\omega'_k \sim \nabla l_k(X_i) - \nabla l_{\hat{k}(X_0)}(X_i)$ is evaluated	$\nabla l_k(X_i) - \nabla l_{\hat{k}(X_0)}(X_i)$
SparseFool [51]	Based on DeepFool. $X^{\text{adv}} = X + r, r = X_i - X_0.$ X_i is iteratively obtained via $X_{i+1} = \text{LinearSolver}(x_i, \omega_i, X_i^B, Q),$ where $X_i^B = X_i + \text{DeepFool}(X_i)$ and $\omega_i = \nabla l_{k(X_i^B)}(X_i^B) - \nabla l_{\hat{k}(X_i)}(X_i^B)$	$\nabla l_{k(X_i^B)}(X_i^B) - \nabla l_{\hat{k}(X_i)}(X_i^B)$

- [16] P. Benz, C. Zhang, A. Karjauv, and I. S. Kweon, "Robustness may be at odds with fairness: An empirical study on class-wise accuracy," in *NeurIPS 2020 Workshop on Pre-registration in Machine Learning*, ser. Proceedings of Machine Learning Research, L. Bertinetto, J. F. Henriques, S. Albanie, M. Paganini, and G. Varol, Eds., vol. 148. PMLR, 11 Dec 2021, pp. 325–342. [Online]. Available: <https://proceedings.mlr.press/v148/benz21a.html>
- [17] S. A. Morcos, G. T. D. Barrett, C. N. Rabinowitz, and M. Botvinick, "On the importance of single directions for generalization," in *International Conference on Learning Representations*, 2018.
- [18] D. Su, H. Zhang, H. Chen, J. Yi, P.-Y. Chen, and Y. Gao, "Is robustness the cost of accuracy? – a comprehensive study on the robustness of 18 deep image classification models," in *Computer Vision – ECCV 2018*, 2018, pp. 644–661.
- [19] P. Arcaini, A. Bombarda, S. Bonfanti, and A. Gargantini, "Roby: a tool for robustness analysis of neural network classifiers," in *2021 14th IEEE Conference on Software Testing, Verification and Validation (ICST)*, 2021, pp. 442–447.
- [20] H. Zhang, Y. Yu, J. Jiao, E. Xing, L. E. Ghaoui, and M. Jordan, "Theoretically principled trade-off between robustness and accuracy," in *Proceedings of the 36th International Conference on Machine Learning*, ser. Proceedings of Machine Learning Research, vol. 97, 09–15 Jun 2019, pp. 7472–7482. [Online]. Available: <https://proceedings.mlr.press/v97/zhang19p.html>
- [21] J. I. Goodfellow, J. Shlens, and C. Szegedy, "Explaining and harnessing adversarial examples," in *International Conference on Learning Representations*, 2015.
- [22] D. Tsipras, S. Santurkar, L. Engstrom, A. Turner, and A. Madry, "Robustness may be at odds with accuracy," in *International Conference on Learning Representations*, 2019.
- [23] J. M. Colbrook, V. Antun, and C. A. Hansen, "The difficulty of computing stable and accurate neural networks: On the barriers of deep learning and smale's 18th problem," *Proceedings of the National Academy of Sciences*, p. e2107151119, 2021.
- [24] Y.-Y. Yang, C. Rashtchian, H. Zhang, R. R. Salakhutdinov, and K. Chaudhuri, "A closer look at accuracy vs. robustness," in *Advances in Neural Information Processing Systems*, H. Larochelle, M. Ranzato, R. Hadsell, M. F. Balcan, and H. Lin, Eds., vol. 33. Curran Associates, Inc., 2020, pp. 8588–8601. [Online]. Available: <https://proceedings.neurips.cc/paper/2020/file/61d77652c97ef636343742fc3dcf3ba9-Paper.pdf>
- [25] E. Arani, F. Sarfraz, and B. Zonooz, "Adversarial concurrent training: Optimizing robustness and accuracy trade-off of deep neural networks," in *The British Machine Vision Conference (BMVC)*, 2020.
- [26] V. Schwag, S. Mahloujifar, T. Handina, S. Dai, C. Xiang, M. Chiang, and P. Mittal, "Improving adversarial robustness using proxy distributions," in *ICLR 2021 Workshop on Security and Safety in Machine Learning Systems*, 2021.
- [27] K. Leino, Z. Wang, and M. Fredrikson, "Globally-robust neural networks," in *International Conference on Machine Learning*, vol. 139, 2021, pp. 6212–6222.
- [28] V. Antun, F. Renna, C. Poon, B. Adcock, and C. A. Hansen, "On instabilities of deep learning in image reconstruction and the potential costs of ai," *Proceedings of the National Academy of Sciences*, pp. 30 088–30 095, 2020.
- [29] A. Rozsa, M. Günther, and E. T. Boult, "Are accuracy and robustness correlated?" in *2016 15TH IEEE International Conference on Machine Learning and Applications (ICMLA 2016)*, 2016, pp. 227–232.
- [30] G. Cybendo, "Approximations by superpositions of a sigmoidal function," *Mathematics of Control, Signals and Systems*, pp. 303–314, 1992.
- [31] K. Hornik, M. Stinchcombe, and H. White, "Multilayer feedforward networks are universal approximators," *Neural Networks*, vol. 2, no. 5, pp. 359–366, 1989. [Online]. Available: <https://www.sciencedirect.com/science/article/pii/0893608089900208>
- [32] E. Gelenbe, "Random Neural Networks with Negative and Positive Signals and Product Form Solution," *Neural Computation*, vol. 1, no. 4, pp. 502–510, 12 1989. [Online]. Available: <https://doi.org/10.1162/neco.1989.1.4.502>
- [33] E. Gelenbe, Z.-H. Mao, and Y.-D. Li, "Function approximation with spiked random networks," *IEEE Transactions on Neural Networks*, vol. 10, no. 1, pp. 3–9, Jan 1999.
- [34] N. Bohr, "On the notions of causality and complementarity," *Science*, vol. 111, no. 2873, pp. 51–54, jan 1950.
- [35] A. Krizhevsky, "Learning multiple layers of features from tiny images," 2009.
- [36] J.-J. Zhang, D.-X. Zhang, J.-N. Chen, and L.-G. Pang, "Robust and Test accuracy of the IFA pipeline and the frequencies related," 2021. [Online]. Available: <https://doi.org/10.7910/DVN/FKFJZQ>
- [37] M. Zhao, X. Dai, B. Wang, F. Yu, and F. Wei, "Further understanding towards sparsity adversarial attacks," in *Advances in Artificial Intelligence and Security*, X. Sun, X. Zhang, Z. Xia, and E. Bertino, Eds. Cham: Springer International Publishing, 2022, pp. 200–212.
- [38] C. Zhang, P. Benz, C. Lin, A. Karjauv, J. Wu, and I. S. Kweon, "A survey on universal adversarial attack," in *Proceedings of the Thirtieth International Joint Conference on Artificial Intelligence, IJCAI-21*, Z.-H. Zhou, Ed. International Joint Conferences on Artificial

- Intelligence Organization, 8 2021, pp. 4687–4694, survey Track. [Online]. Available: <https://doi.org/10.24963/ijcai.2021/635>
- [39] W. Heisenberg, “Über den anschaulichen inhalt der quantentheoretischen kinematik und mechanik,” *Zeitschrift für Physik*, vol. 43, no. 3-4, pp. 172–198, mar 1927.
- [40] A. Agarwal, R. Singh, and M. Vatsa, “The role of ‘sign’ and ‘direction’ of gradient on the performance of cnn,” in *2020 IEEE/CVF Conference on Computer Vision and Pattern Recognition*, 2020, pp. 2748–2756.
- [41] Y. LeCun, B. Boser, J. S. Denker, D. Henderson, R. E. Howard, W. Hubbard, and L. D. Jackel, “Backpropagation applied to handwritten zip code recognition,” *Neural Computation*, vol. 1, no. 4, pp. 541–551, 1989.
- [42] Y. LeCun, L. Bottou, Y. Bengio, and P. Haffner, “Gradient-based learning applied to document recognition,” *Proceedings of the Institute of Radio Engineers*, vol. 86, no. 11, pp. 2278–2323, 1998.
- [43] W. L. Zhang, K. Doi, M. L. Giger, R. M. Nishikawa, and R. A. Schmidt, “An improved shift-invariant artificial neural network for computerized detection of clustered microcalcifications in digital mammograms.” *Medical physics*, vol. 23 4, pp. 595–601, 1996.
- [44] K. He, X. Zhang, S. Ren, and J. Sun, “Deep residual learning for image recognition,” in *2016 IEEE Conference on Computer Vision and Pattern Recognition (CVPR)*, 2016, pp. 770–778.
- [45] C. Szegedy, W. Liu, Y. Jia, P. Sermanet, S. Reed, D. Anguelov, D. Erhan, V. Vanhoucke, and A. Rabinovich, “Going deeper with convolutions,” in *2015 IEEE Conference on Computer Vision and Pattern Recognition (CVPR)*, 2015, pp. 1–9.
- [46] <https://www.kaggle.com/code/yassineghouzam/introduction-to-cnn-keras-0-997-top-6>.
- [47] A. Kurakin, J. I. Goodfellow, and S. Bengio, “Adversarial examples in the physical world,” in *International Conference on Learning Representations*, 2017.
- [48] A. Madry, A. Makelov, L. Schmidt, D. Tsipras, and A. Vladu, “Towards deep learning models resistant to adversarial attacks,” in *International Conference on Learning Representations*, 2018. [Online]. Available: <https://openreview.net/forum?id=rjzIBfZAb>
- [49] N. Papernot, P. McDaniel, S. Jha, M. Fredrikson, Z. B. Celik, and A. Swami, “The limitations of deep learning in adversarial settings,” in *2016 IEEE European Symposium on Security and Privacy (EuroS&P)*, 2016, pp. 372–387.
- [50] S.-M. Moosavi-Dezfooli, A. Fawzi, and P. Frossard, “Deepfool: A simple and accurate method to fool deep neural networks,” in *2016 IEEE Conference on Computer Vision and Pattern Recognition (CVPR)*, 2016, pp. 2574–2582.
- [51] A. Modas, S.-M. Moosavi-Dezfooli, and P. Frossard, “Sparsefool: A few pixels make a big difference,” in *2019 IEEE/CVF Conference on Computer Vision and Pattern Recognition (CVPR)*, 2019, pp. 9079–9088.
- [52] J. Su, D. V. Vargas, and K. Sakurai, “One pixel attack for fooling deep neural networks,” *IEEE Transactions on Evolutionary Computation*, vol. 23, no. 5, pp. 828–841, 2019.
- [53] M. Andriushchenko, F. Croce, N. Flammarion, and M. Hein, “Square attack: A query-efficient black-box adversarial attack via random search,” in *Computer Vision – ECCV 2020*, A. Vedaldi, H. Bischof, T. Brox, and J.-M. Frahm, Eds. Cham: Springer International Publishing, 2020, pp. 484–501.

On The Uncertainty Principle of Neural Networks: Supplementary Material

— Understanding the uncertainty principle in terms of FGSM attack

Jun-Jie Zhang, Dong-Xiao Zhang, Jian-Nan Chen, Long-Gang Pang, and Deyu Meng

Abstract

In this supplementary material, we provide a perspective to understand the uncertainty principle of neural networks proposed in the main paper in terms of the frequency-principle. Based on the observation that an opposite direction of the FGSM attack increases both the Test Accuracy (TA) and Robust Accuracy (RA), we specifically build a pipeline named the Iterative FGSM Augmentation (IFA). In IFA, to obtain high TA and RA is equivalent to train a Pix2Pix network, which maps an image to another image, to high accuracy. Our experiments show that such an attempt to train a Pix2Pix fails at producing images containing more high frequency components. The results indicate that one can hardly expect to train a network (e.g., Pix2Pix) which resolves both the images and their conjugates to an arbitrary high accuracy simultaneously.



Since the Test Accuracy (TA) and Robust Accuracy (RA) of a neural network involve two procedures, it is hard to perceive the uncertainty principle directly. Thus, we provide another view to further perceive the principle.

1 OBSERVATION FOR OBTAINING ACCURATE AND ROBUST NETWORKS

In image classification, a well-trained neural network separates the data points (images) into several classes. If the FGSM attack decreases the classification accuracy, one will be able to attain an increase in accuracy following the opposite direction of the FGSM attack (the same phenomenon is also observed by the current literatures [1], [2]). To intuitively perceive the phenomenon, we schematically depict the effects of both the FGSM attack and its opposite in Fig. 1. The shaded areas correspond to the domains of different image classes which are determined by the loss function. The FGSM attack shifts the data points that belong to the TRUE domain towards other domains so as to attack the classification network. On the contrary, if we iteratively apply the FGSM attack in the opposite direction, we can move these data points back to their TRUE domain classes—thus inclining to gain an augmentation of the accuracies for the training set [1], [2].

To further instantiate the phenomenon, we iteratively apply the opposite FGSM attack via the formula

$$\begin{aligned} X_{n+1} &= X_n - \epsilon \cdot \text{sign}(\nabla_{Xl}(f(X, \theta), Y^*)|_{X=X_n}) \\ &\equiv X_n + D_n, \end{aligned} \quad (1)$$

where X_n and X_{n+1} denote the images before and after the iteration. The relevant TA and RA for images X_{n+1} at different iteration steps are shown in Fig. 2, where we can see that with the increase of the iteration steps, both TA and RA show tendency of increase. Note that in order to obtain X_{n+1} , we need to evaluate the term $\epsilon \cdot \text{sign}(\nabla_{Xl}(f(X, \theta), Y^*)|_{X=X_n})$ which requires to pre-know the label knowledge Y^* . Hence, the opposite FGSM attack is only applicable on the training set so far.

The above phenomena is somehow inspiring. Specifically, it motivates a natural idea that if we can design similar procedures on the test set, we will increase both TA and RA simultaneously, and the deduced uncertainty principle in the paper tends to be doubtful, and we will have actually found a method to defend the adversarial attacks.

2 THE PIPELINE OF THE ITERATIVE FGSM AUGMENTATION

To achieve the goal, we may think of building a Pix2Pix [3], [4] network which aims to learn a mapping to directly output a proper conjugate Δ_N from an input image X_0 , where

$$\begin{aligned} \Delta_N &\equiv X_N - X_0 \\ &= X_{N-1} + D_{N-1} - X_0 = \dots = \sum_{n=0}^{N-1} D_n. \end{aligned} \quad (2)$$

- J.-J. Zhang, D.-X. Zhang and J.-N. Chen are with the Division of Computational physics and Intelligent modeling, Northwest Institute of Nuclear Technology, Shaanxi, Xi'an 710024, China
E-mail: zjacob@mail.ustc.edu.cn
- L.-G. Pang is with the Key Laboratory of Quark & Lepton Physics of Ministry of Education, Central China Normal University, Wuhan 430079, China.
- D. Meng is with School of Mathematics and Statistics and Ministry of Education Key Lab of Intelligent Networks and Network Security, Xi'an Jiaotong University, Shaanxi, P. R. China.
Email: dymeng@mail.xjtu.edu.cn

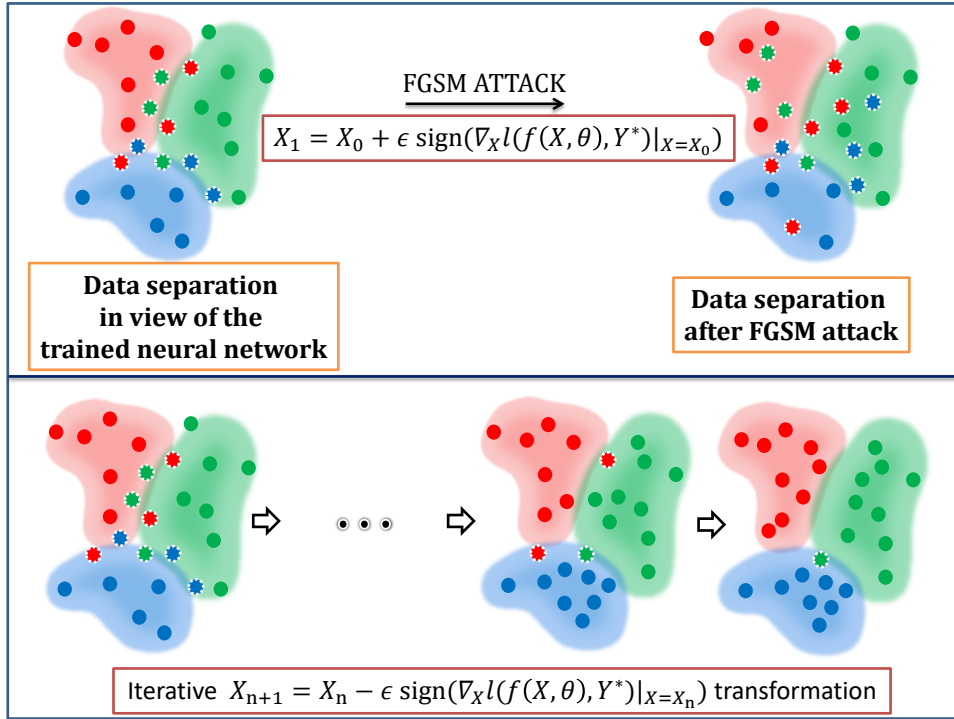


Fig. 1. Illustration of the FGSM attack and its opposite. The upper panel: FGSM attack transforms some of the images (data points) that belong to a certain domain towards other domains, leading to a decrease of the accuracy. The lower panel: the opposite direction of the FGSM attack transforms the images towards the domains with correct classification, leading to an increase of the accuracy.

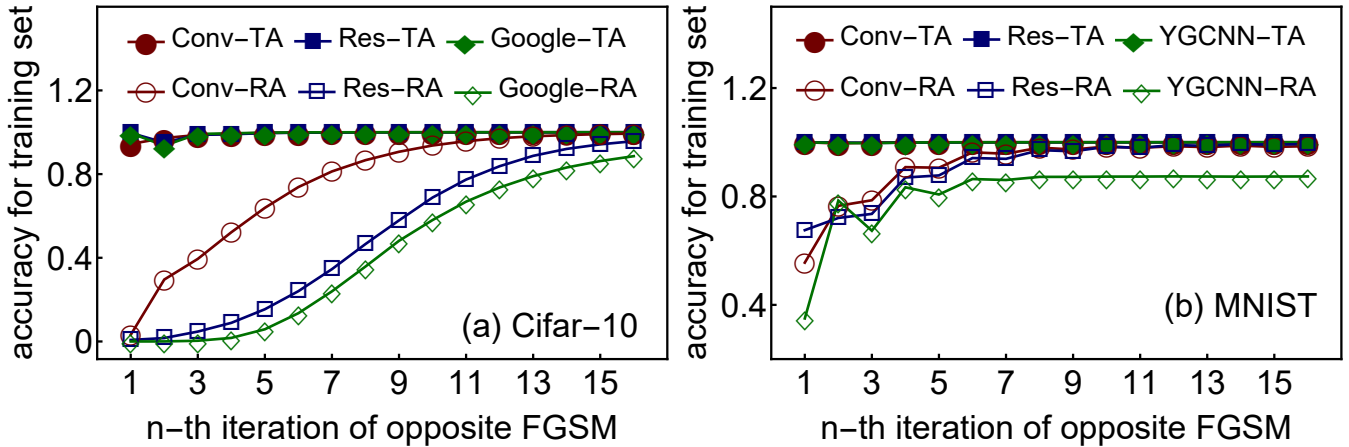


Fig. 2. Test accuracy (TA) and robust accuracy (RA) for training set. ConvNet, ResNet and GoogleNet are applied to the Cifar-10 dataset; and ConvNet, ResNet and YGCNN are applied to the MNIST dataset. The attacking strength $\epsilon = 8/255$ and 0.1 for Cifar-10 and MNIST respectively. The detailed structures of these networks can be found in Ref. [3]

The capital N represents the final iteration number through Eq. (1). Δ_N can be seen as a conjugate of the raw image X_0 . With such a network, we can obtain the corresponding Δ_N with given X_0 . Once Δ_N is obtained, we can immediately construct X_N via $X_N = X_0 + \Delta_N$. According to Fig. 2, X_N so obtained is expected to pose both high TA and high RA in terms of the trained classifier. We name this conjecture as Iterative FGSM Augmentation (IFA, see Fig. 3 for details). The IFA algorithm aims to connect the X_0 and its conjugate Δ_N in one single network by adopting the Pix2Pix network.

The purpose of this design is to substantiate that the Pix2Pix network cannot resolve X_0 and its conjugate Δ_N to an arbitrary high accuracy simultaneously, so as to further validate that the RA and TA cannot get sufficiently better at the same time. The uncertainty principle of neural networks can then be more faithfully verified. As will be shortly revealed, due to the uncertainty principle of neural networks, such an ideal Pix2Pix network can hardly achieve its intended purpose.

3 MANIFESTATION OF THE UNCERTAINTY PRINCIPLE

Now we can follow the four steps in IFA attempting to train such an ideal Pix2Pix network that generates Δ_N providing the raw images X_0 .

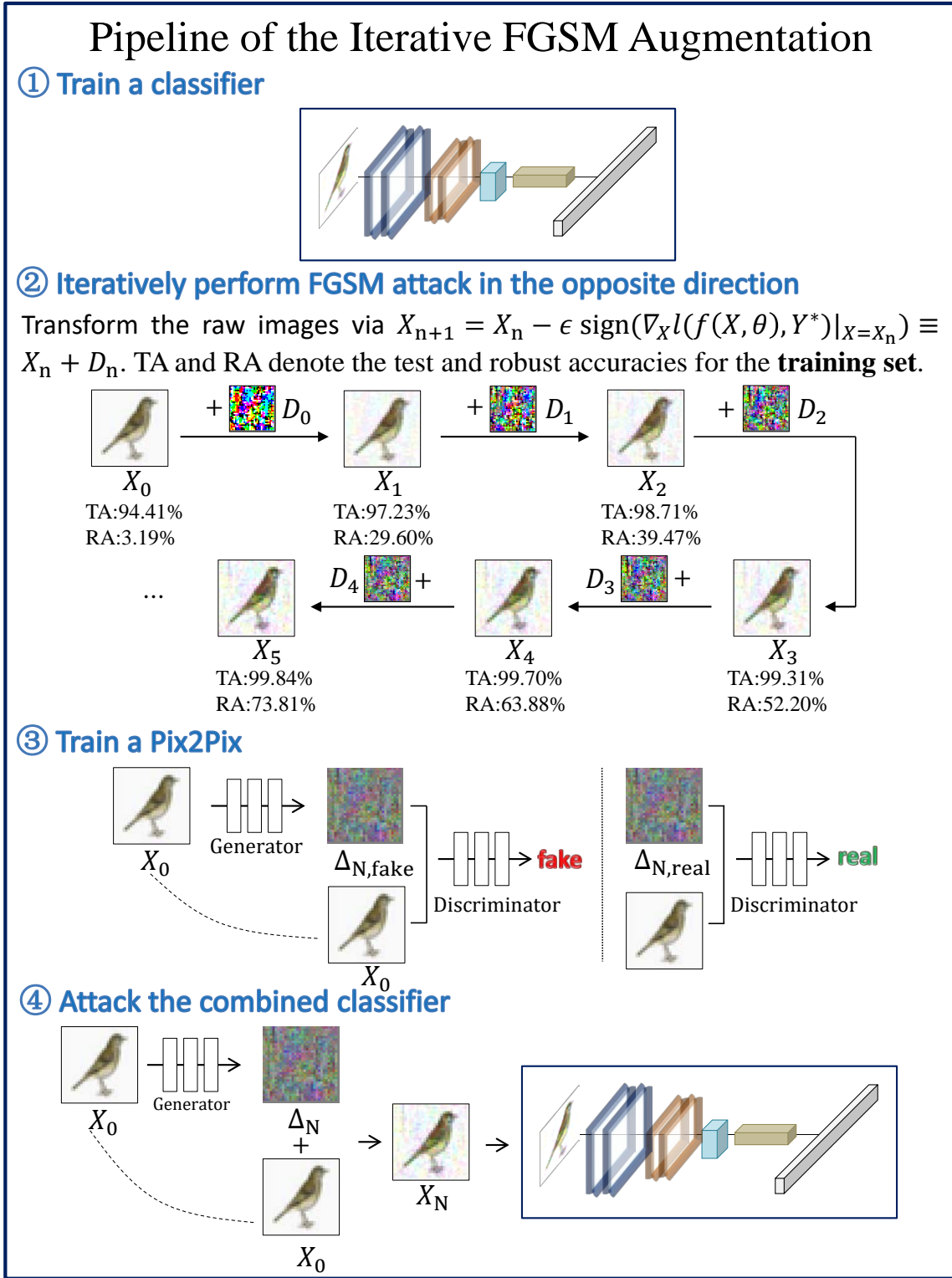


Fig. 3. The pipeline of the iterative FGSM augmentation. ① A classifier (for instance the Residual neural network) is first trained with N_{epoch} epoches, where X_0 and Y^* , denote the raw images and labels. ② Based on the observation that the opposite direction of the FGSM attack increases the accuracy, we iteratively perform the FGSM attack in the opposite direction so as to increase the test accuracies (TA) and robust accuracies (RA) of the training set. Hence, as long as one obtains Δ_N for image X_0 , $X_0 + \Delta_N$ will have both high TA and RA. ③ For the test set, since the label Y^* is unknown, Δ_N cannot be obtained directly. Instead, we construct a Pix2Pix network whose inputs are X and outputs are Δ_N . ④ Providing the images X_0 (in the test set) to the Pix2Pix generator, we gain its conjugation Δ_N and X_N . Then, we evaluate the relevant TA and RA for images X_N . Note that RA is obtained via the iterative FGSM attack (with step size 4 and l_∞ loss) applied to the combined neural network (Pix2Pix+classifier).

TABLE 1

Test and robust accuries for the classifiers on MNIST dataset. CL stands for classifiers that are not combined with a Pix2Pix network and ACL stands for the classifiers Pix2Pix+Conv/Res/YGCNN.

Network type		Test accuracy (%)			Robust accuracy (%)		
		N_{epoch}			N_{epoch}		
		1	30	50	1	30	50
ConvNet	CL	97.31	98.71	98.72	41.44	50.98	53.74
	ACL	99.04	98.87	99.25	89.53	93.90	98.00
ResNet	CL	98.65	99.50	99.57	90.88	98.22	98.27
	ACL	99.32	99.15	89.85	95.44	52.96	51.03
YGCNN	CL	97.35	99.15	99.19	59.84	49.06	45.68
	ACL	98.96	99.08	98.29	95.43	89.95	67.73

First of all, we train a few classifiers on the datasets Cifar-10 and MNIST at various epoch numbers (denoted as N_{epoch}). In general larger N_{epoch} values correspond to more accurate classifiers. Here, we use the typical Convolutional (ConvNet), Residual (ResNet), Google (GoogleNet) networks for Cifar-10 dataset and train these networks with epoch numbers $N_{\text{epoch}} = 1, 5, 50$. For MNIST dataset, we use the ConvNet, ResNet, and YGCNN [5] (proposed by YASSINE GHOUZAM) networks. Since the MNIST dataset is much easier compared with the Cifar-10, TA for $N_{\text{epoch}} = 5$ will be similar to that of $N_{\text{epoch}} = 1$. To observe prominent effects, the classifiers for MNIST are trained with $N_{\text{epoch}} = 1, 30, 50$. Once these classifiers are obtained, we can evaluate their TA and RA to see how robust the classifiers can be. For convenience, we refer the obtained TA and RA in this stage to CL, meaning the normal classifier learning (CL) without iterative FGSM augmentation.

Then we perform the second step of IFA. Since the classifiers are already trained, we can use Eqs. (1) and (2) to generate Δ_N iteratively. The maximum iteration step is chosen to be $N = 200$. Generally, TA and RA for X_n will increase with the increasing of n . In step one, we have chosen three epoch numbers for each classifier. Thus, we obtain three different sets of the training weights. For example, for ConvNet on Cifar-10, we have trained weights $\theta_{N_{\text{epoch}}=1}$, $\theta_{N_{\text{epoch}}=5}$, and $\theta_{N_{\text{epoch}}=50}$. For each weight, for instance $\theta_{N_{\text{epoch}}=5}$, we can generate Δ_{200} using Eq. (1) and (2). This procedure can form a new dataset where (X_0, Δ_{200}) are the (input, label) pairs. At this stage, we have generated a dataset containing both the inputs X_0 and the relevant conjugates Δ_{200} .

Next, we train a Pix2Pix network with training sample pairs (X_0, Δ_{200}) following the third step of IFA. The training of Pix2Pix is an independent procedure which is irrelevant to the classifiers in step one, and does not alter the weights of the classifiers. The Pix2Pix network used here is a Generative Adversarial Network (GAN) with a U-Net structure containing 5 convolutional blocks as the encoder, and 4 deconvolutional layers as the decoder. Each convolutional block is a combination of 2 convolutional layers. The discriminator of the Pix2Pix consists of three convolutional blocks, where each convolutional block contains 1 convolutional layer with spectral normalization, 1 batch normalization layer and 1 leakyReLU layer. The specific implementation of the Pix2Pix and the classifiers can be found in Ref. [3].

Once trained, the Pix2Pix can be used to directly produce the conjugate information Δ_{200} on the test set (the last step of IFA). With the generated Δ_{200} , we are able to further construct images $X_{200} = X_0 + \Delta_{200}$ and use the classifiers trained in step one to evaluate the corresponding TA and RA. Note that in the last step of IFA, we do not change the weights of the classifiers; and RA is obtained by attacking the augmented classifiers (ACL) Pix2Pix+Conv/Res/Google/YGCNN using PGD. Thus, the PGD here attacks both the Pix2Pix network and the classifiers.

In Tab. 1, we present the obtained TA and RA on MNIST dataset. From the uncertainty relation Eq. (14) in the main manuscript, we know that there exists a lower bound which is directly related to the loss function; and the values of the loss function depends on the architecture of the network and the dataset. Thus, whether one can increase TA and RA for a trained classifier simultaneously depends on both the network architecture and the dataset. The results in Tab. 1 can be interpreted in terms of two aspects:

1. If, the classifier does not reach the lower bound, it is possible for us to increase both its TA and RA, as is illustrated by the ConvNet in Tab. 1.

2. Since the test accuracy often increases with the growing epoch numbers, in some cases, the lower bound in the uncertainty relation will only be reached at relatively larger epoch numbers. Under these circumstances, one is able to increase both TA and RA at small epoch numbers while fail at larger epoch numbers. Meanwhile, the conditions for larger epoch numbers also have two folds: we cannot increase both TA and RA (the ResNet case), or we can increase RA in sacrifice of decreasing TA (the YGCNN case).

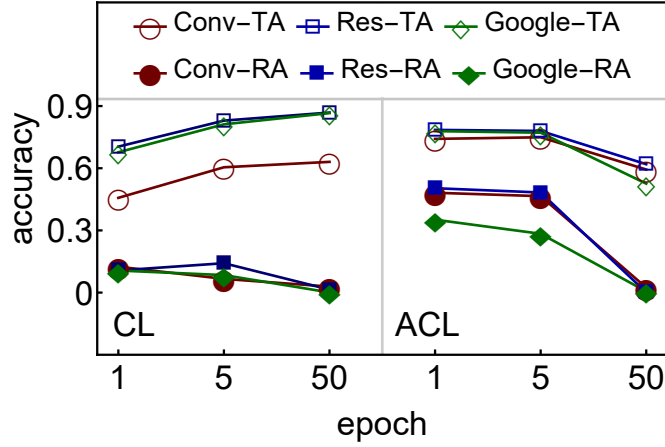


Fig. 4. Test and robust accuracies of the classifiers on Cifar-10 dataset. CL stands for classifiers that are not combined with a Pix2Pix network and ACL stands for the classifiers Pix2Pix+Conv/Res/Google. Other parameters are set the same to Fig. 2.

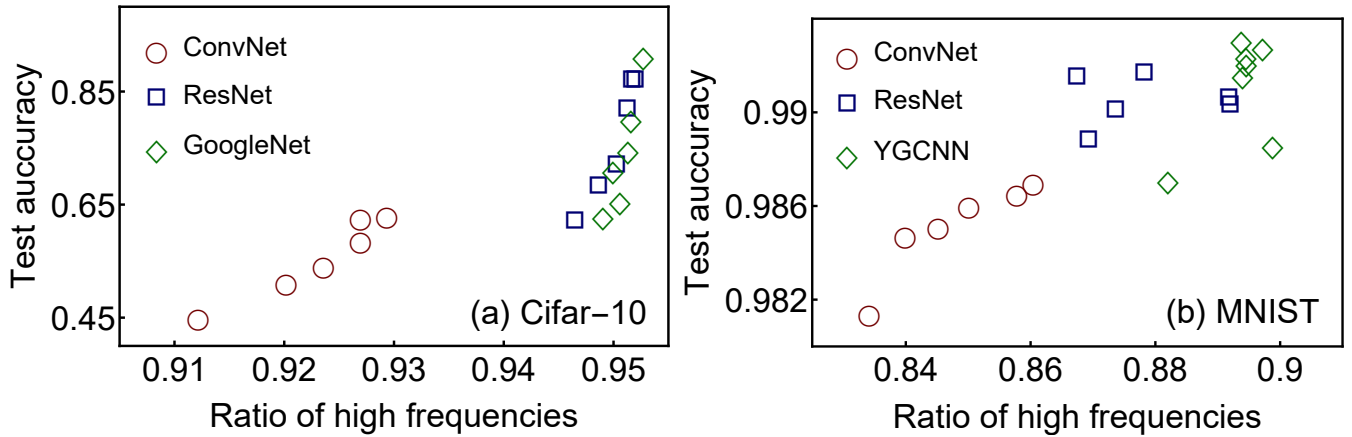


Fig. 5. Ratio of high frequencies is roughly proportional to the test accuracies. Ratio of high frequencies is obtained via the formula $(|\text{FFT}[\Delta_1]| - |\text{FFT}[\Delta_1]_{LF}|) / |\text{FFT}[\Delta_1]|$. For Cifar-10, we turn the RGB images into gray and $|\text{FFT}[\Delta_1]_{LF}|$ takes the slices $[15 : 19, 15 : 19]$. For MNIST, $|\text{FFT}[\Delta_1]_{LF}|$ takes the slices $[12 : 18, 12 : 18]$. The networks are trained with various epoch numbers to gain the different test accuracies. The implementation can be found in Ref. [3].

The similar phenomenon is also observed on Cifar-10. In Fig. 4 we give the TA and RA for classifiers ConvNet, ResNet and GoogleNet. In this scenario, an increase in TA corresponds to a decrease in RA in general, as clearly depicted in the left panel of Fig. 4, indicating that there is a trade-off between TA and RA. For the combined classifiers (Pix2Pix+Conv/Res/Google), TA and RA both decrease (Fig. 4 right panel) with the increasing of the epoch number N_{epoch} , indicating that the IFA pipeline fails at increasing TA and RA simultaneously.

In general, we see that we can hardly train a Pix2Pix network to an arbitrary high accuracy. Meanwhile, we also observe a decrease of TA and RA for ACL in some cases. This decreasing tendency manifests the difficulty for the Pix2Pix to generate ideal conjugate Δ_{200} .

Note that the core of the IFA pipeline is that we have combined the images and their conjugates in a single network (the generator in Pix2Pix). If the uncertainty principle is not an inherent property for all neural networks, we are able train the Pix2Pix network to arbitrary high accuracies, so that an increase of TA and RA should be observed. However, our attempt has failed so far, indicating the existence of such an uncertainty principle.

Since the Pix2Pix network directly links the inputs and the corresponding conjugates, the statement in uncertainty principle that "a neural network cannot resolve the inputs and the corresponding conjugates to arbitrary high accuracies" is now converted into "such Pix2Pix neural network cannot generate Δ_N with given X to an arbitrary high accuracy". To this extent, we have converted a classifier into a generator, thus we state that the uncertainty principle should be a common result for general neural networks.

4 THE FREQUENCY-PRINCIPLE EXPLANATION

Apart from the uncertainty principle, the results presented in Fig. 4 can also be understood from the frequency-principle [6] (F-Principle) in a straightforward way. It is proposed by the F-Principle that "the DNNs tend to fit training data by a low-frequency function resulting from the smoothness/regularity of the commonly used activation functions". Therefore,

it is harder for the neural networks to predict high-frequency images than the low-frequency ones. To be specific, in the training of reducing the loss function $l(f(X, \theta), Y^*)$, smaller values of l indicate higher training (and also test) accuracies if the network is not over fitted. For a network to distinguish among many classes, high-frequency features are gradually resolved in the training course. Thus, a neural network with higher accuracy contains more high-frequency features [7], [8]. In Fig. 5, we compare the test accuracies of the classifiers with the proportion of the high frequencies of the generated Δ_1 . We see that Δ_1 contains more high frequency components with the increasing of the test accuracies, and Δ_1 with more high frequencies is more difficult for a Pix2Pix network to produce.

Therefore, a more accurate classifier should generate the Δ_1 with higher frequencies. Meanwhile, a robust classifier corresponds to the generation (by Pix2Pix) of Δ_1 to high precision, which is harder to achieve if Δ_1 contains more high frequency components. This can rationally explain the phenomenon that both TA and RA decrease with N_{epoch} in Fig. 4.

REFERENCES

- [1] J. I. Goodfellow, J. Shlens, and C. Szegedy, "Explaining and harnessing adversarial examples," in *International Conference on Learning Representations*, 2015.
- [2] A. Agarwal, R. Singh, and M. Vatsa, "The role of 'sign' and 'direction' of gradient on the performance of cnn," in *2020 IEEE/CVF Conference on Computer Vision and Pattern Recognition*, 2020, pp. 2748–2756.
- [3] J.-J. Zhang, D.-X. Zhang, J.-N. Chen, L.-G. Pang, and D. Meng, "Robust and Test accuracy of the IFA pipeline and the frequencies related," 2021. [Online]. Available: <https://doi.org/10.7910/DVN/FKFJZQ>
- [4] P. Isola, J.-Y. Zhu, T. Zhou, and A. A. Efros, "Image-to-image translation with conditional adversarial networks," in *2017 IEEE Conference on Computer Vision and Pattern Recognition (CVPR)*, 2017, pp. 5967–5976.
- [5] <https://www.kaggle.com/code/yassineghouzam/introduction-to-cnn-keras-0-997-top-6>.
- [6] J. Z.-Q. Xu, Y. Zhang, T. Luo, Y. Xiao, and Z. Ma, "Frequency principle: Fourier analysis sheds light on deep neural networks," *Communications in Computational Physics*, pp. 1746–1767, 2020.
- [7] J. Z.-Q. Xu, Y. Zhang, and Y. Xiao, "Training behavior of deep neural network in frequency domain," in *Neural Information Processing (ICONIP 2019)*, 2019, pp. 264–274.
- [8] H. Wang, X. Wu, Z. Huang, and P. E. Xing, "High-frequency component helps explain the generalization of convolutional neural networks," *2020 IEEE/CVF Conference on Computer Vision and Pattern Recognition (CVPR)*, pp. 8681–8691, 2020.